

Adaptive Optimization via Momentum on Variance-Normalized Gradients

Francisco Patitucci[†] Aryan Mokhtari^{†,‡}

[†]UT Austin [‡]Google Research

Abstract

We introduce MVN-Grad (*Momentum on Variance-Normalized Gradients*), an Adam-style optimizer that improves stability and performance by combining two complementary ideas: variance-based normalization and momentum applied *after* normalization. MVN-Grad scales each coordinate by an exponential moving average of gradient uncertainty and applies momentum to the resulting normalized gradients, eliminating the cross-time coupling between stale momentum and a stochastic normalizer present in standard Adam-type updates. We prove that this decoupling yields strictly smaller one-step conditional update variance than momentum-then-normalize variance methods under standard noise assumptions, and that MVN-Grad is robust to outliers: it has a uniformly bounded response to single gradient spikes. In low-variance regimes, we further show variance normalization avoids sign-type collapse associated with second-moment scaling and can yield accelerated convergence. Across CIFAR-100 image classification and GPT-style language modeling benchmarks, MVN-Grad matches or outperforms Adam, AdaBelief, and LaProp, delivering smoother training and improved generalization with no added overhead.

1 Introduction

Adaptive gradient methods such as Adam [KB14] are widely used in modern deep learning due to their empirical robustness and ease of hyperparameter tuning. Predecessors like AdaGrad [DHS11] and RMSProp [HSS12] pioneered the use of coordinate-wise preconditioning based on running statistics. Adam builds on these foundations by combining an exponential moving average (EMA) of gradients with per-coordinate normalization based on the second moment, enabling rapid convergence across diverse architectures. Despite their success, a growing body of work has identified failure modes and generalization limitations of Adam-type methods in stochastic optimization [WRSSR17; RKK19; CLSH18]. We identify two fundamental structural limitations in the Adam design that contribute to these failures: temporal coupling and suboptimal scaling.

First, a critical weakness lies in Adam’s standard *momentum-then-normalize* ordering, which creates a stochastic coupling between the numerator and denominator. While both terms utilize EMAs, their interaction induces a temporal mismatch. The momentum term m_t acts as a heavy memory buffer for *past* gradients, whereas the adaptive denominator is continuously modulated by the *current* stochastic gradient g_t . This creates a risk of “cross-time” instability: if the normalizer transiently dips—for instance, during a mini-batch with low gradient magnitude—while the momentum buffer still retains a large value from a past outlier, the effective step size can explode. This coupling amplifies stale gradients and distorts the update direction, a failure mode that has been also highlighted in some recent work [ZHU20; ZZLWZY18; ZDTD21].

Second, reliance on the *uncentered second moment* for normalization can lead to ineffective scaling, since $\mathbb{E}[g_t^2] = (\mathbb{E}[g_t])^2 + \text{Var}(g_t)$ mixes signal and noise. In low-variance regimes where the signal dominates, the normalizer tracks the squared gradient magnitude, causing the adaptive term to scale the gradient by roughly its own size ($g_t/\sqrt{g_t^2} \approx \text{sign}(g_t)$) and degenerate into a coordinate-wise sign operation. This “sign collapse” discards scale information, forcing uniform step sizes regardless of local curvature and significantly slowing convergence in high-signal regimes [BH18; BWAA18].

Prior attempts to improve Adam address these design axes in isolation, effectively trading one limitation for another. To resolve the temporal mismatch, LaProp [ZHU20] applies momentum to the *normalized* gradient, while AdaShift [ZZLWZY18] decorrelates numerator and denominator via temporally shifted statistics. Although these methods decouple history from current noise, they retain the second-moment normalizer and remain susceptible to sign collapse. Conversely, AdaBelief [ZDTD20] adopts variance-based scaling but ignores the ordering flaw; because variance estimates are smaller and more volatile than second moments, the standard ordering can make them less stable than Adam [YG20]. Consequently, the design space remains fragmented, forcing a choice between structural stability and adaptive sensitivity.

Contributions. We introduce MVN-Grad (Momentum on Variance-Normalized Gradients), which addresses two key limitations via a *normalize-then-momentum* structure and variance-based normalization. Applying momentum *after* normalization removes stochastic coupling and improves stability when the normalizer fluctuates, while replacing the second moment with a variance estimate avoids sign collapse and preserves gradient scale in high-signal regimes.

- **Theoretical Stability Analysis.** We prove that the *normalize-then-momentum* ordering yields strictly smaller one-step conditional update variance than standard variance-based methods like AdaBelief (Theorem 3.1). We further establish robustness to outliers: we show that MVN-Grad produces uniformly bounded updates even under arbitrarily large gradient spikes (Theorem 3.2).
- **Convergence in High-Signal Regimes.** We characterize the limitations of second-moment normalization in low-noise settings. We show that while methods like LaProp degenerate into

Algorithm 1 MVN-Grad (Momentum on Variance-Normalized Gradients)

Require: step size η , $\beta_1, \beta_2 \in [0, 1]$, $\varepsilon > 0$, $\varepsilon_s \geq 0$

- 1: Initialize $m_0 \leftarrow 0$, $s_0 \leftarrow 0$, $u_0 \leftarrow 0$, parameters x_0
- 2: **for** $t = 1, 2, \dots$ **do**
- 3: $g_t \leftarrow \nabla_x f(x_{t-1}; \xi_t)$
- 4: $m_t \leftarrow \beta_1 m_{t-1} + (1 - \beta_1) g_t$
- 5: $s_t \leftarrow \beta_2 s_{t-1} + (1 - \beta_2) (g_t - m_t)^2 + \varepsilon_s$
- 6: $c_m \leftarrow 1 - \beta_1^t$; $c_v \leftarrow 1 - \beta_2^t$
- 7: $z_t \leftarrow g_t / (\sqrt{\frac{s_t}{c_v}} + \varepsilon)$
- 8: $u_t \leftarrow \beta_1 u_{t-1} + (1 - \beta_1) z_t$
- 9: $x_t \leftarrow x_{t-1} - \eta u_t / c_m$
- 10: **end for**

coordinate-wise sign updates (“sign-collapse”), MVN-Grad’s variance-based scaling preserves gradient magnitude information. We prove that this property avoids the dimension-dependent slowdowns suffered by sign-based methods (Theorem 3.3).

- **Empirical Performance.** We evaluate MVN-Grad against established baselines including Adam(W), AdaBelief, and LaProp on standard benchmarks such as image classification (ResNet on CIFAR-10/100) and language modeling (GPT-2 on OpenWebText) [HZRS16; KH+09; RW-CLAS+19; Kar22]. Our experiments show that MVN-Grad consistently matches or outperforms these methods.

Additional related work. A large body of work has proposed Adam variants targeting stability and convergence (e.g., AMSGrad [RKK19], Yogi [ZRSKK18], RAdam [LJHCLGH19]), practical training refinements (e.g., AdamW [LH+17], AdaFactor [SS18]), or stronger preconditioning (e.g., Sophia [LLHLM23], AdaHessian [YGSMMK21]). These methods address complementary aspects of adaptive optimization; we review them in Appendix A.

2 Proposed Algorithm

Consider the stochastic optimization of a differentiable function $F(x)$, where at iteration t we observe a stochastic gradient $g_t = \nabla_x f(x_{t-1}; \xi_t)$ with $\xi_t \sim \mathcal{D}$. Updates are element-wise; for readability, we present the scalar form.

We introduce *Momentum on Variance-Normalized Gradients* (MVN-Grad), an Adam-style optimizer defined by two complementary choices: (i) variance-based normalization and (ii) applying momentum *after* normalization. Concretely, MVN-Grad replaces Adam’s second-moment EMA normalizer with a variance estimator, and it applies momentum to the normalized gradients rather than normalizing the momentum itself. We first state the MVN-Grad update, then explain these two ingredients, and finally position MVN-Grad relative to other adaptive methods.

The procedure is summarized in Algorithm 1. After computing the stochastic gradient g_t (Line 3), we update a gradient EMA, m_t , in Line 4. Crucially, this m_t serves solely to center the second moment for the variance estimation in Line 5. Specifically, s_t tracks the moving average of the squared deviations between g_t and m_t , acting as a variance proxy. In Line 7, we use the bias-corrected s_t to normalize the current gradient, generating the normalized direction z_t . Finally, we compute the momentum of this normalized sequence, storing it in u_t (Line 8), and use its bias-corrected version to update the parameters in Line 9.

Remark 2.1. In Algorithm 1, we use the same decay rate β_1 for both the gradient mean estimator m_t (Line 4) and the momentum buffer u_t (Line 8) to avoid introducing an extra hyperparameter and to remain consistent with standard Adam-style interfaces. However, these updates serve distinct roles: m_t estimates the gradient center for variance computation, while u_t accumulates the update direction. Decoupling them with a separate decay rate may be advantageous in non-stationary settings where variance estimation and momentum evolve on different timescales.

Remark 2.2. To stabilize steps where the instantaneous variance estimate $(g_t - m_t)^2$ is extremely small, we add a constant ε_s during the variance accumulation step (Line 5). This induces a lower bound on the proxy s_t , thereby limiting the effective normalization magnitude in Line 7. While our theoretical analysis assumes $\varepsilon_s = 0$ for simplicity, practical implementations often benefit from $\varepsilon_s > 0$ to prevent numerical instability.

Taxonomy of Adaptive Architectures. Adaptive methods can be categorized along two orthogonal axes. The first axis is the choice of *normalizer*. Standard methods track the uncentered second moment $v_t \approx \mathbb{E}[g_t^2]$, whereas variance-based methods track the centered second moment $s_t \approx \text{Var}(g_t)$. Let $\text{EMA}_\beta(x_t)$ denote the exponential moving average of a sequence x_t with decay β . Using momentum m_t as the mean estimate, the normalizers are:

$$v_t = \text{EMA}_{\beta_2}(g_t^2) \quad \text{vs} \quad s_t = \text{EMA}_{\beta_2}((g_t - m_t)^2). \quad (1)$$

The second axis is the *ordering* of operations. Let $r_t \in \{v_t, s_t\}$ denote the chosen normalizer. *Momentum-then-normalize* methods aggregate gradients before scaling, while *normalize-then-momentum* methods scale the instantaneous gradient before aggregation. Ignoring bias corrections, these distinct update directions can be written as:

$$\Delta_t^{\text{pre}} = \frac{\text{EMA}_{\beta_1}(g_t)}{\sqrt{r_t} + \varepsilon} \quad \text{vs} \quad \Delta_t^{\text{post}} = \text{EMA}_{\beta_1} \left(\frac{g_t}{\sqrt{r_t} + \varepsilon} \right). \quad (2)$$

In the first case (Δ_t^{pre}), the EMA is applied to the raw gradient g_t . In the second case (Δ_t^{post}), the EMA acts on the normalized gradient, serving as the final operation.

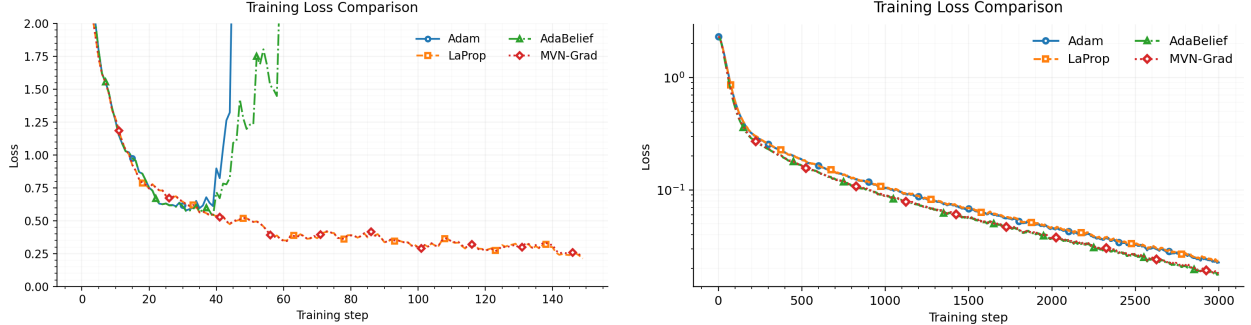
These choices define a complete 2×2 design space. The *momentum-then-normalize* form (Δ_t^{pre}) includes Adam with second-moment scaling ($r_t = v_t$) and AdaBelief with variance scaling ($r_t = s_t$). The *normalize-then-momentum* form (Δ_t^{post}) includes LaProp, which retains second-moment scaling, and MVN-Grad, which uniquely combines variance normalization with post-normalization momentum.

Why the two axes matter. As highlighted, MVN-Grad differs from Adam along two design axes: the choice of normalizer and the ordering of operations. These axes address distinct failure modes of adaptive optimization and are therefore complementary. We next provide a high-level motivation for these modifications and formalize the resulting guarantees in Section 3.

(A) Choosing the ordering. Swapping the order of normalization and applying momentum changes the *temporal dependency* of the update. Standard momentum-then-normalize methods (like Adam and AdaBelief) divide the momentum buffer m_t by the current normalizer r_t . Since $m_t = \beta_1 m_{t-1} + (1 - \beta_1) g_t$ contains both past and current gradients, the update can be decomposed as:

$$\Delta_t^{\text{pre}} = \frac{\beta_1 m_{t-1}}{\sqrt{r_t} + \varepsilon} + \frac{(1 - \beta_1) g_t}{\sqrt{r_t} + \varepsilon}.$$

The first term divides a history-dependent quantity m_{t-1} by the present-time statistic r_t , creating a risky “cross-time” ratio. If the normalizer transiently dips (e.g., the current batch is low-noise)



(a) MVN-Grad produces smoother dynamics and reduced loss spikes relative to Adam-style baselines. Full hyperparameter settings are provided in Appendix C.1.

(b) Training loss on MNIST for a 2-layer MLP with batch size 1024. In low-variance regimes, variance-based normalization preserves gradient scale, yielding faster convergence than second-moment methods. Experimental details are in Appendix C.1.

Figure 1: MNIST training loss for different batch sizes. Full hyperparameters in Appendix C.1.

while the momentum buffer still reflects a past spike, this contribution can be artificially amplified. In contrast, normalize-then-momentum forms the ratio $g_t/\sqrt{r_t}$ at the *same timestep*, ensuring the gradient is stabilized *before* entering the momentum buffer and eliminating this specific coupling; as illustrated by the toy example in Figure 1a.

Importantly, this behavior is not merely heuristic. This structural change yields two formal stability gains. First, as proved in Section 3.1, applying momentum after normalization strictly reduces the one-step conditional variance by eliminating the stochastic interaction between carry-over momentum and a random denominator. Second, this ordering ensures that isolated gradient spikes are clipped immediately, a property formalized in Section 3.2. Unlike Adam, where spikes are stored and re-emitted over many steps, MVN-Grad scales outliers at the source.

(B) Choosing the normalizer. Switching from the second-moment normalizer v_t to the variance proxy s_t changes the *scale* of the update. The second moment mixes signal and noise and scales with $\mathbb{E}[g_t^2] \approx \mu^2 + \sigma^2$, whereas the variance s_t isolates the noise level σ^2 . This distinction is especially pronounced in low-variance regimes ($\sigma \ll \mu$), which are illustrated by the toy example in Figure 1b. In such settings, second-moment normalization effectively rescales the gradient by its own magnitude ($g_t/\sqrt{v_t} \approx g_t/|g_t|$), causing the method to collapse to a conservative, sign-based update. In contrast, variance normalization scales deviations around the mean, preserving informative gradient magnitudes up to a noise-dependent preconditioner. Importantly, this behavior is not merely anecdotal: as we formally prove in Section 3.3, variance-based methods achieve fast convergence in low-noise regions, whereas second-moment methods incur dimension-dependent slowdowns.

3 Theoretical Guarantees

This section rigorously justifies the design choices above. We first formalize the stability gains of the *normalize-then-momentum* ordering by establishing a conditional variance gap, showing that it yields strictly smaller update variance than standard methods under common noise assumptions. We then analyze robustness to outliers in demonstrating that applying momentum after normalization prevents divergence of update moments. Then, we study the *variance-based normalizer* in low-noise regimes, showing that it avoids sign collapse and enables faster convergence.

Before presenting our results, we fix notation. We analyze the optimization coordinate-wise

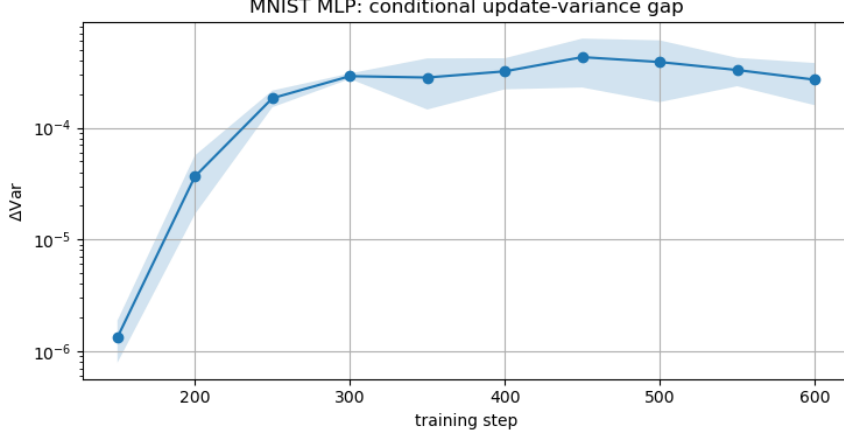


Figure 2: Conditional update-variance gap, estimated by Monte Carlo at frozen checkpoints and averaged over three seeds.

and let g_t denote the stochastic gradient at step t for a fixed coordinate. All random variables are defined on a filtered probability space $(\Omega, \mathcal{F}, (\mathcal{F}_t)_{t \geq 0}, \mathbb{P})$, where \mathcal{F}_{t-1} captures the history up to time $t-1$. Let $\mu_t := \mathbb{E}[g_t | \mathcal{F}_{t-1}]$ denote the conditional mean. For clarity, we omit bias-correction factors of the form $1/(1 - \beta^t)$, as they do not affect our conclusions. We denote the update directions for Adam and AdaBelief by Δ_t^A and Δ_t^{AB} , corresponding to the *pre-normalization* structure Δ_t^{pre} in (2) with $r_t = v_t$ and $r_t = s_t$ from (1), respectively. Likewise, LaProp and MVN-Grad are denoted by Δ_t^{LP} and Δ_t^{MV} , corresponding to the *post-normalization* structure Δ_t^{post} with $r_t = v_t$ and $r_t = s_t$, respectively.

3.1 Conditional variance comparison

We quantify the stability gain of applying momentum *after* normalization while using the same variance proxy s_t . Specifically, we compare the one-step *conditional update variance* of AdaBelief and MVN-Grad, $\text{Var}(\Delta_t^{AB} | \mathcal{F}_{t-1})$ versus $\text{Var}(\Delta_t^{\text{MV}} | \mathcal{F}_{t-1})$. This conditional variance measures the unpredictability of the next update given the past, with smaller values indicating smoother dynamics. Under a standard symmetry assumption on centered gradient noise and an idealized mean-tracking condition on the EMA, the variance gap has a closed form and is always nonnegative.

Theorem 3.1. *Assume that, conditional on \mathcal{F}_{t-1} , the centered gradient $g_t - \mu_t$ is symmetric, where $\mu_t := \mathbb{E}[g_t | \mathcal{F}_{t-1}]$. Assume moreover that the EMA tracks the conditional mean, i.e., $m_{t-1} = \mu_t$. Define $\Delta\text{Var}_t := \text{Var}[\Delta_t^{AB} | \mathcal{F}_{t-1}] - \text{Var}[\Delta_t^{\text{MV}} | \mathcal{F}_{t-1}]$. Then*

$$\Delta\text{Var}_t = (2\beta_1 - \beta_1^2) m_{t-1}^2 \text{Var}\left(\frac{1}{\sqrt{s_t + \varepsilon}} \mid \mathcal{F}_{t-1}\right) \geq 0.$$

Theorem 3.1 isolates a concrete stability difference between the two update rules. Even when both methods use the same variance proxy s_t , AdaBelief carries past information through the term $m_{t-1}/(\sqrt{s_t} + \varepsilon)$: it multiplies the previous momentum estimate m_{t-1} by the current random normalizer. This introduces a stochastic coupling between the carry-over term and the instantaneous variance estimate, and yields an extra conditional-variance contribution proportional to $m_{t-1}^2 \text{Var}((\sqrt{s_t} + \varepsilon)^{-1} | \mathcal{F}_{t-1})$. In contrast, MVN-Grad applies momentum to already-normalized

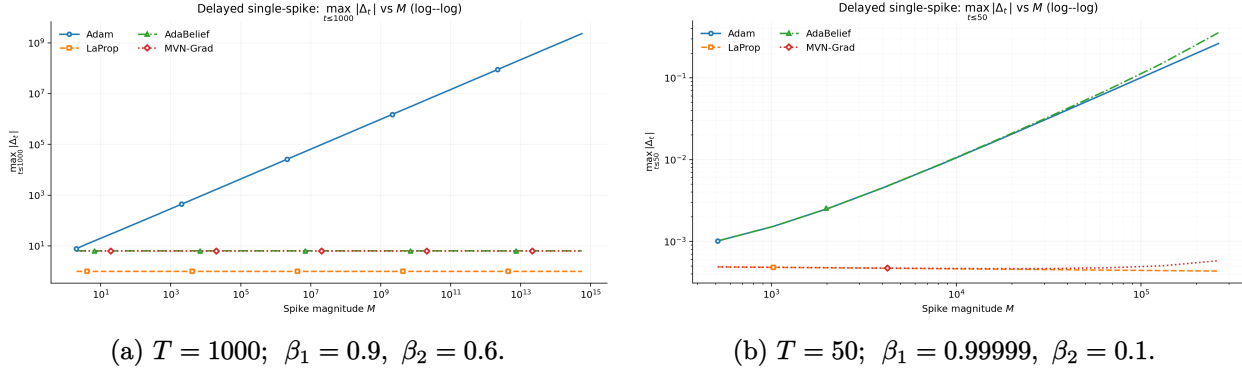


Figure 3: Delayed single-spike robustness: peak update magnitude $\max_{0 \leq \tau \leq T} |\Delta_\tau|$ versus spike size M (log–log). Within each panel, all optimizers use the same hyperparameters. Experimental details are in Appendix C.2.

gradients, so its carry-over term is \mathcal{F}_{t-1} -measurable and does not interact with the randomness of $(\sqrt{s_t} + \varepsilon)^{-1}$ at time t . As conditional variance quantifies the variability of the update given the past, this gap corresponds to less predictable one-step updates for AdaBelief under the same normalizer. The symmetry and mean-tracking assumptions in Theorem 3.1 enable an explicit closed-form gap. More generally, the same mechanism persists without exact symmetry or perfect mean tracking: the conditional variance difference depends on whether carry-over momentum is multiplied by a *random* normalizer at time t . This interaction arises in AdaBelief but disappears when momentum is applied after normalization, since the carry-over term is then \mathcal{F}_{t-1} -measurable.

To empirically validate Theorem 3.1, we estimate the one-step conditional update variance along a real training trajectory. We train a two-hidden-layer MLP on MNIST using AdaBelief and MVN-Grad (batch size 16, learning rate 10^{-3} , $\beta_1 = 0.9$, $\beta_2 = 0.95$) and record the variance gap at selected checkpoints. At each checkpoint, we freeze the optimizer state $(x_{t-1}, m_{t-1}, s_{t-1})$ and evaluate both methods from the *same* state by drawing $K = 128$ independent mini-batches. Using the resulting gradients, we form one-step updates for AdaBelief and MVN-Grad and estimate $\Delta \text{Var}(t) = \text{Var}(\Delta_t^{\text{AB}} \mid \mathcal{F}_{t-1}) - \text{Var}(\Delta_t^{\text{MV}} \mid \mathcal{F}_{t-1})$ via Monte Carlo. Variances are computed coordinate-wise, averaged over parameters, and then over three seeds. Across all checkpoints, the estimated conditional variance gap is positive on average as shown in Figure 2.

3.2 Single-spike robustness

To make the ordering effect in Section 3.1 concrete, we consider a simple outlier model in which the gradient has a single large spike at initialization and is otherwise well behaved. This setup isolates whether a one-time outlier is absorbed by the adaptive normalizer or stored in momentum and later re-emitted as an oversized update. The key takeaway is that normalize–then–momentum methods remain uniformly bounded in the spike magnitude, whereas momentum–then–normalize methods can retain spike effects through the momentum state, leading to spike-dependent responses as formalized for Adam in Theorem 3.2 and illustrated empirically for AdaBelief in Figure 3.

Theorem 3.2. *Consider the single-spike model $g_0 = Mu$ for $M \gg 1$ and $u \neq 0$, and $g_t = u$ for all $t \geq 1$. Assume the EMA initializations satisfy $v_{-1} = s_{-1} = \bar{d} > 0$ and $\varepsilon > 0$. For LaProp and MVN-Grad, the update magnitudes are uniformly bounded:*

$$|\Delta_t^{\text{LP}}| \leq C, \quad |\Delta_t^{\text{MV}}| \leq C, \quad \forall t \geq 0,$$

where C depends only on $(\beta_1, \beta_2, \bar{d}, u, \varepsilon)$ and not on M . In contrast, for Adam if we define $t^* := \min \{t \geq 1 : (1 - \beta_2)\beta_2^t M^2 \leq 1\}$, then there exists $c > 0$, depending only on $(\beta_1, \beta_2, \bar{d}, u, \varepsilon)$, such that

$$|\Delta_{t^*}^A| \geq c(1 - \beta_1)\beta_1^{t^*} M.$$

Theorem 3.2 formalizes a sharp contrast in how a spike propagates through the optimizer state. For Adam, the spike enters the raw momentum m_0 and decays as $\beta_1^t M$, while the second-moment accumulator v_t forgets the spike as $\beta_2^t M^2$. At the time t^* when the spike contribution in v_t has returned to the baseline scale, Adam can still retain a nonnegligible carry-over term in the numerator, yielding a spike-dependent update of order $(1 - \beta_1)\beta_1^{t^*} M$. In contrast, LaProp and MVN-Grad apply momentum to normalized gradients: the spike is scaled by the adaptive denominator at $t = 0$, and the resulting momentum cannot reintroduce a factor that grows with M . Thus, applying momentum *after* normalization prevents a single outlier from being stored and replayed. This carry-over effect does not contradict the classical gradient-independent upper bound on Adam's update in the regime $\beta_2 > \beta_1^2$. In that regime, the uniform bound prevents spike-induced growth, and the lower bound in Theorem 3.2 may be loose. We clarify this regime dependence in Remark 3.1.

We corroborate these predictions with simulations under the single-spike model. We set $g_0 = Mu$ for fixed $u \neq 0$, followed by $g_t = u$ for all $t \geq 1$, and initialize the EMAs with $m_{-1} = 0$ and $v_{-1} = s_{-1} = \bar{d} > 0$. For each configuration, we simulate T iterations and record the peak update magnitude $\max_{0 \leq \tau \leq T} |\Delta_\tau|$ as a function of M . Figure 3a uses $T = 1000$ with $(\beta_1, \beta_2) = (0.9, 0.6)$, while Figure 3b uses $T = 50$ with $(\beta_1, \beta_2) = (0.99999, 0.1)$ to emphasize early carry-over effects. Consistent with Theorem 3.2, LaProp and MVN-Grad exhibit an $O(1)$ response in M , while Adam shows pronounced spike-dependent growth. We also include AdaBelief: in the regime of Figure 3a it remains bounded, whereas in the regime of Figure 3b it can display spike-dependent amplification. Note that a formal spike analysis for AdaBelief is more involved due to the coupling between its variance estimator and the momentum state, so we focus on empirical behavior instead.

Remark 3.1. If $\beta_2 > \beta_1^2$, then Adam admits a gradient-independent upper bound: $|\Delta_t^A| \leq \frac{1 - \beta_1}{\sqrt{1 - \beta_2}} \cdot \frac{1}{\sqrt{1 - \beta_1^2/\beta_2}}$ for all $t \geq 0$. In this regime, no choice of gradients can cause unbounded amplification of the normalized update. On the other hand, Theorem 3.2 identifies a structural carry-over effect in the momentum-then-normalize ordering. Once the spike is stored in m_0 , at the “forgetting time” t^* (when the spike contribution in v_t returns to the baseline scale) the numerator can still retain a remnant on the order of $(1 - \beta_1)\beta_1^{t^*} M$. Theorem 3.2 holds for all (β_1, β_2) ; however, when $\beta_2 > \beta_1^2$, the fact that t^* grows logarithmically with M implies that $\beta_1^{t^*}$ decays with M , preventing this remnant from yielding an M -growing update and rendering the lower bound potentially loose. Outside this regime (e.g., $\beta_1 \approx 1$ with smaller β_2), the remnant can translate into pronounced spike-dependent growth over practical ranges of M , as illustrated in Fig. 3.

3.3 Second moment vs. variance normalization

The preceding subsections showed robustness to outliers and heavy-tailed noise. We now consider a complementary low-variance regime common in later training, where gradients align closely with the signal. In this setting, we compare second-moment and variance-based normalizers via the update directions they induce. The second moment mixes signal and noise, scaling as $\mathbb{E}[g_t^2] = (\mathbb{E}[g_t])^2 + \text{Var}(g_t)$, whereas the variance isolates the noise. When $\text{Var}(g_t) \ll (\mathbb{E}[g_t])^2$, second-moment normalization becomes overly conservative and collapses toward sign-based updates, while variance normalization preserves magnitude information up to an inverse-noise preconditioner.

To formalize this intuition, we adopt a standard approximation from the analysis of exponential moving averages. Over the effective averaging window of length $(1 - \beta_2)^{-1}$, we assume the gradient distribution varies slowly, allowing the stochastic gradient to be decomposed into a deterministic signal and a noise term with slowly varying second-order statistics. Under this locally stationary approximation, the bias-corrected exponential moving averages act as estimators of the gradient's second moment and variance. This assumption does not require global stationarity, only moment stability over the EMA window.

Assumption 3.1. *At iteration t , the stochastic gradient admits the decomposition $g_t = \nabla F(x_{t-1}) + \xi_t$, where $\mathbb{E}[\xi_t | \mathcal{F}_{t-1}] = 0$ and $\text{Var}(\xi_{t,i} | \mathcal{F}_{t-1}) \approx \sigma_i^2$ remains approximately constant over the EMA window. The estimators satisfy $\mathbb{E}[v_{t,i}] \approx \nabla_i F(x_{t-1})^2 + \sigma_i^2$ and $\mathbb{E}[s_{t,i}] \approx \sigma_i^2$.*

Under Assumption 3.1, both LaProp and MVN-Grad admit the coordinate-wise recursion $x_t = x_{t-1} - \eta u_t$, where $u_t = \beta_1 u_{t-1} + (1 - \beta_1)z_t$, but they differ in the normalized direction z_t , i.e.,

$$z_t^{\text{LP}} = \text{sign}(g_t) \sqrt{\frac{1}{(1 + \frac{v_t - g_t^2}{g_t^2})}}, \quad z_t^{\text{MV}} = \frac{g_t}{\sqrt{s_t}}.$$

Thus, the comparison reduces to characterizing these directions in the low-variance regime. To isolate the effect of the normalizer and suppress stochastic fluctuations, we formalize this regime as follows.

Assumption 3.2 (Small variance relative to signal). *Along the trajectory, $g_t \approx \nabla_i F(x_{t-1})$ and $\sigma_i^2 \ll \nabla_i F(x_{t-1})^2$.*

Under Assumptions 3.1–3.2, the two normalization schemes admit distinct deterministic limits. We analyze them in turn. For LaProp, which uses second-moment normalization, the EMA satisfies $v_t \approx \nabla_i F(x_{t-1})^2$. As a result, the corrective factor obeys $\sqrt{\frac{1}{1 + (v_t - g_t^2)/g_t^2}} \approx 1$,

and the normalized direction reduces to $z_t^{\text{LP}} \approx \text{sign}(g_t) \approx \text{sign}(\nabla_i F(x_{t-1}))$. Thus, in the low-variance regime, LaProp behaves like a momentum-smoothed sign method and largely discards gradient magnitude information. In contrast, MVN-Grad uses variance normalization, for which \hat{s}_t estimates the coordinate-wise variance σ_i^2 . When this estimate is stable and strictly positive on the EMA time scale, the normalized direction satisfies $z_t^{\text{MV}} = \frac{g_t}{\sqrt{s_t}} \approx \frac{\nabla_i F(x_{t-1})}{\sigma_i}$. Consequently, MVN-Grad preserves gradient magnitudes up to an inverse-noise preconditioner and avoids collapse to a sign direction. Although the above discussion applies broadly, focusing on smooth objectives allows a precise separation and sharp convergence rates in low-variance regimes.

Theorem 3.3. *Let F be L -smooth and bounded below on \mathbb{R}^d , and suppose Assumptions 3.1–3.2 hold. In addition, assume a high-SNR stochastic oracle: $g_t = \nabla F(x_{t-1}) + \xi_t$ with $\mathbb{E}[\xi_t | \mathcal{F}_{t-1}] = 0$, and for some $\delta \in (0, 1)$ and $\sigma \geq 0$, $|\xi_{t,i}| \leq \delta |\nabla_i F(x_{t-1})|$ a.s. and $\mathbb{E}[\xi_{t,i}^2 | \mathcal{F}_{t-1}] \leq \sigma^2 \forall i$.*

(i) (MVN-Grad, upper bound.) *Assume isotropic noise $\sigma_i = \sigma > 0$ for all i and a stable variance estimate $s_t \approx \sigma^2 \mathbf{1}$ along the trajectory, so that the limiting MVN-Grad direction satisfies $z_t^{\text{MV}} \approx g_t/\sigma$. Define $\alpha := \eta(1 - \beta_1)/\sigma$ and assume $\alpha \leq (1 - \beta_1^2)/L$. Then it suffices to take $T = \mathcal{O}(1/\varepsilon^2)$ iterations to ensure $\min_{0 \leq t \leq T} \mathbb{E} \|\nabla F(x_t)\|_2 \leq \varepsilon$.*

(ii) (LaProp, lower bound.) *There exists an L -smooth function F (satisfying the same assumptions and oracle model above) and an initialization such that, in the low-variance phase where $z_t^{\text{LP}} \approx \text{sign}(g_t)$, the following holds. For LaProp with step size $\eta_t = \frac{c}{L\sqrt{t+1}}$, achieving $\min_{0 \leq t \leq T} \|\nabla F(x_t)\|_2 \leq \varepsilon$ requires $T = \Omega\left(\frac{d}{\varepsilon^2}\right)$ iterations.*

Table 1: CIFAR-100 / ResNet-18, batch size 128: accuracy (mean \pm std over 3 seeds) for the selected configuration.

Optimizer	Test Accuracy	Train Accuracy
Adam	77.82 ± 0.18	75.65 ± 0.71
LaProp	77.72 ± 0.20	75.59 ± 0.99
AdaBelief	79.93 ± 0.15	81.22 ± 0.88
MVN-Grad	79.94 ± 0.17	81.26 ± 0.94

Table 2: CIFAR-100 / ResNet-18, batch size 1024: accuracy (mean \pm std over 3 seeds) for the selected configuration.

Optimizer	Test Accuracy	Train Accuracy
Adam	78.26 ± 0.14	83.15 ± 1.28
LaProp	78.40 ± 0.14	83.05 ± 1.34
AdaBelief	79.34 ± 0.27	85.89 ± 1.17
MVN-Grad	79.63 ± 0.12	85.89 ± 1.19

Theorem 3.3 shows a sharp separation between variance-based and second-moment normalization in low-variance regimes. By comparing MVN-Grad and LaProp, two methods that share the same normalize-then-momentum structure, we isolate the effect of the normalizer itself. In this setting, variance normalization yields dimension-free convergence, whereas second-moment normalization induces sign-like dynamics and dimension-dependent slowdown. A similar separation holds for Adam and AdaBelief, though it is confounded by differences in update ordering.

4 Experiments

We compare MVN-Grad with Adam, AdaBelief, and LaProp on two benchmarks: (i) image classification on CIFAR-100 using ResNet-18, and (ii) autoregressive language modeling with GPT-style Transformers on WikiText-103 and OpenWebText. Across all experiments, we fix the model architecture and all non-optimizer hyperparameters and tune only (η, β_1, β_2) and, when applicable, the variance-normalization parameter ε_s . For each benchmark, we first perform a coarse sweep to identify stable learning-rate ranges, followed by a focused sweep over (η, β_1, β_2) and ε_s when applicable. We select the best configuration using one validation seed, then rerun it with multiple seeds and report mean \pm std.

4.1 CIFAR-100 with ResNet-18

We train a ResNet-18 model on CIFAR-100 for 200 epochs using cosine learning-rate decay with warmup, weight decay, RandAugment, MixUp, and label smoothing. We consider batch sizes 128 and 1024 to probe different gradient-noise regimes. For each choice, we allocate the same sweep budget per optimizer over learning rate η and (β_1, β_2) , and (for variance-normalized methods) ε_s . We select the best configuration with one validation seed, then re-run it with three seeds and report mean \pm std; full grids are in Appendix C.3.

Tables 1–2 report final test accuracies for the selected configuration, while Figures 4a, 5a, 4b, and 5b summarize robustness via boxplots over all sweep runs. At batch size 128, MVN-Grad

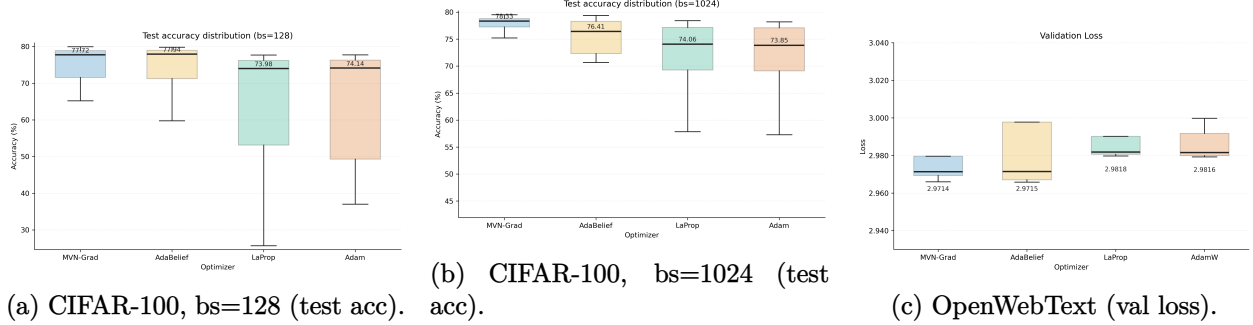


Figure 4: Hyperparameter robustness across sweep runs (*validation*): (a) CIFAR-100 bs=128, (b) CIFAR-100 bs=1024, (c) OpenWebText.

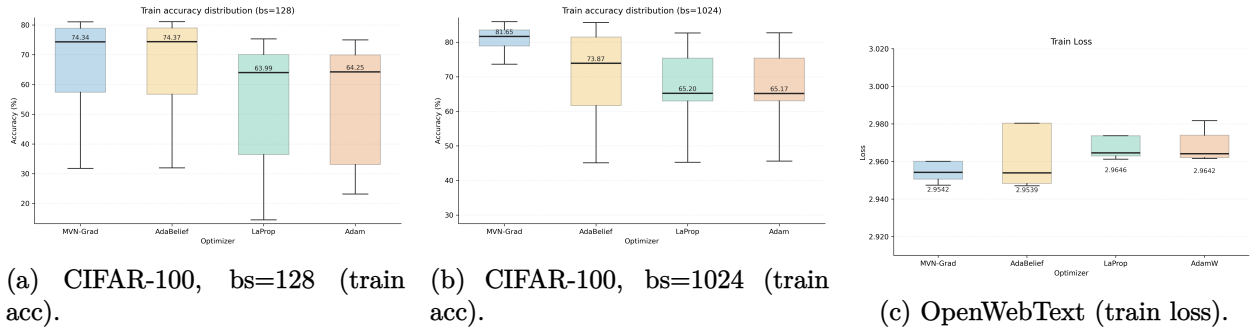


Figure 5: Hyperparameter robustness across sweep runs (*training*): (a) CIFAR-100 bs=128, (b) CIFAR-100 bs=1024, (c) OpenWebText.

matches AdaBelief and improves over Adam and LaProp by about 2.1–2.2% test accuracy, with comparable sweep medians (e.g., 77.72% vs. 77.94% test accuracy) and noticeably shorter left tails than Adam and LaProp. At batch size 1024, MVN-Grad achieves the best mean test accuracy (79.63%), improving over AdaBelief by 0.29% while matching its train accuracy (85.89%), and also exhibits the strongest robustness in the sweeps: its boxplots are shifted toward higher accuracy with a markedly improved lower tail, yielding the highest median test accuracy (78.33% vs. 76.41% for AdaBelief and $\approx 74\%$ for Adam and LaProp) and the highest median train accuracy (81.65% vs. 73.87% for AdaBelief and $\approx 65\%$ for Adam and LaProp).

4.2 Language modeling

We evaluate two GPT-style language modeling benchmarks: a 30M-parameter model on WikiText-103 and a 124M-parameter model on OpenWebText. We evaluate validation negative log-likelihood (NLL) and perplexity $\text{PPL} = \exp(\mathcal{L}_{\text{NLL}})$, using PPL on WikiText-103 and validation loss on OpenWebText for consistency with NanoGPT logging.

WikiText-103 (GPT-2 30M / NanoGPT). We train a 30M-parameter GPT-2-style Transformer with sequence length 512 on WikiText-103. All results are reported as mean \pm standard deviation over 4 seeds. We adopt a two-stage tuning protocol. First, we perform a coarse sweep over learning rates $\{10^{-4}, 10^{-3}, 10^{-2}\}$ with $\beta_1 \in \{0.9, 0.95\}$ and $\beta_2 \in \{0.99, 0.999\}$ to identify stable learning-rate regimes. Final comparisons use a focused sweep in which all optimizers are evaluated on identical grids with learning rates $\{5 \times 10^{-4}, 10^{-3}\}$, $\beta_1 \in \{0.6, 0.7, 0.9, 0.95\}$, and $\beta_2 \in \{0.95, 0.99\}$. Variance-normalized methods additionally evaluate $\varepsilon_s \in \{0, 10^{-8}\}$.

Table 3: WikiText-103 (GPT-2, seq=512), batch size 128: perplexity (mean \pm std over 4 seeds).

Optimizer	Val PPL	Train PPL
Adam	64.50 ± 1.16	71.33 ± 2.55
LaProp	66.96 ± 5.20	73.63 ± 5.09
AdaBelief	63.55 ± 1.11	70.92 ± 1.25
MVN-Grad	62.62 ± 2.52	70.01 ± 3.28

Table 4: OpenWebText (GPT-2, block=1024), micro-batch 12, grad-acc 40 (eff. batch size 480): loss (mean \pm std over 3 seeds) for the selected configuration.

Optimizer	Val Loss	Train Loss
AdamW	2.98970 ± 0.00994	2.97153 ± 0.00866
LaPropW	2.99037 ± 0.01015	2.97202 ± 0.00942
AdaBeliefW	2.97438 ± 0.00811	2.95578 ± 0.00755
MVN-GradW	2.97347 ± 0.00746	2.95520 ± 0.00691

The WikiText-103 experiments use *coupled* ℓ_2 regularization, in which the term λx_{t-1} is added to the stochastic gradient prior to moment estimation. Under coupled decay, the regularization signal is filtered through the optimizer’s internal states, and its effect depends on update ordering—specifically, whether momentum is applied before normalization (Adam, AdaBelief) or after normalization (LaProp and MVN-Grad variants). This interaction can increase seed sensitivity. For the larger-scale OpenWebText experiments below, we instead use *decoupled* weight decay to enable a cleaner comparison. As shown in Table 3, MVN-Grad achieves the best mean validation perplexity. Compared to Adam, MVN-Grad reduces validation perplexity by 1.88, and compared to AdaBelief by 0.93. We observe higher std for LaProp, and to a lesser extent MVN-Grad, in this setting. We do not report boxplots for this sweep: to reduce cost, we early-terminate clearly non-competitive configurations based on intermediate validation performance, so completed runs have varying lengths and do not form a consistent sample of the full grid for each optimizer.

OpenWebText (GPT-2 124M / NanoGPT). We train a GPT-2 124M model on OpenWebText with context length 1024, using micro-batches of size 12 with 40 gradient-accumulation steps (effective batch size 480), bf16 precision, gradient clipping at 1, 2000 warmup steps, and 120k training iterations. We disable dropout and use AdamW-style *decoupled* weight decay with coefficient 0.1 for all methods. For variance-normalized methods we set $\varepsilon_s = 0$. Based on pilot runs, we fix the peak learning rate to $\eta = 10^{-4}$ for all optimizers and tune only (β_1, β_2) . For each optimizer, we evaluate the same nine representative (β_1, β_2) pairs: $(0.6, 0.99)$, $(0.6, 0.999)$, $(0.7, 0.95)$, $(0.7, 0.99)$, $(0.7, 0.999)$, $(0.8, 0.9)$, $(0.8, 0.99)$, $(0.8, 0.999)$, and $(0.9, 0.95)$. We select the configuration minimizing final validation loss and re-run it with three seeds, reporting mean \pm standard deviation.

Table 4 reports final losses for the selected configurations, while Figures 4c–5c visualize robustness via boxplots over all evaluated hyperparameters. MVN-Grad achieves the best mean validation and training losses, slightly improving over AdaBeliefW and more clearly outperforming AdamW and LaPropW. Across the full sweep, MVN-GradW attains the lowest median validation loss (2.9714), improving over AdaBeliefW (2.9715) and outperforming AdamW and LaPropW (both ≈ 2.9816 – 2.9818), with similarly competitive train-loss medians. Moreover, normalize-then-momentum methods (MVN-GradW and LaPropW) show narrower interquartile ranges than momentum-then-normalize baselines, indicating reduced sensitivity to (β_1, β_2) at a fixed learning

rate.

5 Conclusion

We proposed *MVN-Grad*, an Adam-style optimizer that applied momentum *after* variance-based normalization. Our analysis showed this ordering reduced conditional update variance and bounded spike sensitivity; in the small-variance (high-signal) regime it avoided sign-collapse and the resulting dimension-dependent slowdowns. On CIFAR-100 and GPT-style language modeling, MVN-Grad matched or improved over Adam/AdaBelief/LaProp with similar computational cost.

Acknowledgments

This work was supported in part by NSF CAREER Award CCF-2338846 and the NSF AI Institute for Foundations of Machine Learning (IFML). We thank the Center for Generative AI (CGAI) and the Texas Advanced Computing Center (TACC) at The University of Texas at Austin for computing support on the Vista GPU Cluster.

Contents of Appendix

A	Extended related work: Adam-style optimizers	15
B	Theory	16
B.1	Proof of Theorem 3.1	16
B.2	Proof of Theorem 3.2	17
B.3	Proof of Theorem 3.3	19
C	Experiments	24
C.1	MNIST experiment hyperparameters	24
C.2	Single-spike robustness experiment hyperparameters	24
C.3	CIFAR-100 with ResNet-18	24
C.4	Selected LM hyperparameters	25

A Extended related work: Adam-style optimizers

A taxonomy of Adam variants. Most Adam-style optimizers modify (i) the adaptivity statistic and its update rule, (ii) the coupling between numerator and denominator (including update ordering or temporal decorrelation), (iii) step-size control (e.g., bounds or variance rectification), (iv) practical regularization details (e.g., weight decay), and/or (v) systems constraints such as memory footprint or large-batch training.

Convergence and stability fixes. A key theoretical line identifies settings where Adam can fail and proposes convergent variants such as AMSGrad [RKK19]. Related stability-oriented modifications include controlling the growth of second-moment accumulators (Yogi [ZRSKK18]) and rectifying early-stage variance of the adaptive learning rate (RAdam [LJHCLGH19]).

Decoupling momentum and adaptivity. Several methods aim to reduce harmful interactions between historical momentum and stochastic normalization. LaProp [ZWU20] applies momentum after normalization to separate these effects, which is closely related in spirit to our focus on ordering. AdaShift [ZZLWZY18] uses temporally shifted statistics to decorrelate numerator and denominator.

Alternative scaling rules. Beyond second-moment normalization, AdaBelief [ZTDTD20] adapts step sizes using deviations from the predicted gradient. This line targets scaling behavior and can be viewed as variance-sensitive normalization.

Practical refinements and generalization-motivated variants. AdamW [LH+17] decouples weight decay from the gradient step. Memory and implementation constraints motivated AdaFactor [SS18] and SM3 [AGKS19]. Other variants aim to mitigate the adaptivity-generalization gap or extreme effective learning rates via bounded/partial adaptivity, including AdaBound [LXLS19] and Padam [CZTYCG18]. Further modifications address scale-invariant weights (AdamP [HCO-HYKUH20]).

Large-batch and large-scale training. Layer-wise adaptations such as LAMB [YLRHKBS-DKH19] and methods like NovoGrad [GCHKLLNZN19] target stability and efficiency in large-batch regimes.

Interpretations of Adam and sign-like behavior. Several works interpret Adam as combining sign-like directions with variance-dependent magnitudes [BH18], and analyze generalization differences between adaptive methods and SGD [WRSSR17]. These perspectives connect directly to the sign-collapse phenomenon discussed in Section 3.3.

Beyond diagonal second-moment preconditioning. Recent optimizers incorporate curvature information using inexpensive diagonal Hessian estimates and clipping, including Sophia [LLHLM23] and related diagonal-curvature methods such as AdaHessian [YGSKM21]. We include these for context, though they go beyond strictly Adam-style diagonal second-moment preconditioning. Related preconditioning methods include Shampoo [GKS18] and Muon [JJBCNB].

Summary table. For quick reference, Table 5 summarizes representative Adam-style variants, highlighting the core modification each method makes and the primary motivation behind it.

Method(s)	Key change	Main purpose
AMSGrad [RKK19]	Monotone denominator via max-correction	Convergence / avoid pathological steps
Yogi [ZRSKK18], RAdam [LJHCLGH19]	Stabilize/rectify second-moment statistics	Reduce instability (esp. early / heavy variance)
AdaShift [ZZLWZY18]	Time-shifted statistics	Decorrelate numerator and denominator
LaProp [ZWU20]	Momentum <i>after</i> normalization	Reduce coupling of stale momentum and noisy scaling
AdaBelief [ZTDT- DPD20]	Deviation/variance-sensitive scaling	Improve adaptivity when noise is small
AdamW [LH+17]	Decoupled weight decay	Correct regularization under adaptivity
AdaFactor [SS18], SM3 [AGKS19]	Memory-efficient accumulators	Scale to large models / reduced memory
AdaBound [LXLS19], Padam [CZTYCG18]	Bounded/partial adaptivity	Control extreme per-coordinate LRs; SGD-like late stage
AdamP [HCO- HYKUH20]	Projection for scale-invariant parameters	Improve behavior with norm/scale invariances
LAMB [YLRHKBS- DKH19], NovoGrad [GCHKLLNZC19]	Layer-wise scaling / trust ratio	Large-batch stability and efficiency
Sophia [LLHLM23], AdaHessian [YGSMKM21]	Diagonal curvature information	Curvature-aware scaling beyond second moments

Beyond Adam-style diagonal preconditioning (context): Shampoo [GKS18], Muon [JJBJCNB].

Table 5: Representative variants around Adam (not exhaustive).

B Theory

B.1 Proof of Theorem 3.1

Proof. Fix an iteration t and define

$$Y_t := \frac{1}{\sqrt{s_t + \varepsilon}}, \quad X_t := \frac{g_t}{\sqrt{s_t + \varepsilon}} = g_t Y_t.$$

We can write the updates as

$$\Delta_t^{AB} = \beta_1 m_{t-1} Y_t + (1 - \beta_1) X_t,$$

and, since MVN-Grad applies momentum *after* normalization,

$$\Delta_t^{MV} = \beta_1 u_{t-1} + (1 - \beta_1) X_t,$$

where u_{t-1} is \mathcal{F}_{t-1} -measurable.

Conditional variance gap identity. Because m_{t-1} and u_{t-1} are \mathcal{F}_{t-1} -measurable, we have

$$\begin{aligned} \text{Var}[\Delta_t^{AB} \mid \mathcal{F}_{t-1}] &= \text{Var}[\beta_1 m_{t-1} Y_t + (1 - \beta_1) X_t \mid \mathcal{F}_{t-1}] \\ &= \beta_1^2 m_{t-1}^2 \text{Var}[Y_t \mid \mathcal{F}_{t-1}] + (1 - \beta_1)^2 \text{Var}[X_t \mid \mathcal{F}_{t-1}] \\ &\quad + 2\beta_1(1 - \beta_1)m_{t-1} \text{Cov}[Y_t, X_t \mid \mathcal{F}_{t-1}], \end{aligned}$$

and

$$\text{Var}[\Delta_t^{MV} \mid \mathcal{F}_{t-1}] = \text{Var}[\beta_1 u_{t-1} + (1 - \beta_1) X_t \mid \mathcal{F}_{t-1}] = (1 - \beta_1)^2 \text{Var}[X_t \mid \mathcal{F}_{t-1}].$$

Subtracting yields

$$\Delta \text{Var}_t = \beta_1^2 m_{t-1}^2 \text{Var}[Y_t \mid \mathcal{F}_{t-1}] + 2\beta_1(1 - \beta_1)m_{t-1} \text{Cov}[Y_t, X_t \mid \mathcal{F}_{t-1}]. \quad (3)$$

Evaluate the covariance term via symmetry. Let $z := g_t - m_{t-1}$. By assumption, conditional on \mathcal{F}_{t-1} the random variable z is symmetric and centered $\mathbb{E}[z \mid \mathcal{F}_{t-1}] = 0$. Moreover, using the recursion $m_t = \beta_1 m_{t-1} + (1 - \beta_1)g_t$, we have

$$g_t - m_t = \beta_1(g_t - m_{t-1}) = \beta_1 z.$$

Since $s_t = \beta_2 s_{t-1} + (1 - \beta_2)(g_t - m_t)^2$, it follows that

$$s_t = \beta_2 s_{t-1} + (1 - \beta_2)\beta_1^2 z^2, \quad \text{and hence} \quad Y_t = \frac{1}{\sqrt{\beta_2 s_{t-1} + (1 - \beta_2)\beta_1^2 z^2 + \varepsilon}}.$$

Therefore Y_t is an *even* function of z , while zY_t and zY_t^2 are *odd* functions of z . Also,

$$X_t = g_t Y_t = (z + m_{t-1})Y_t.$$

Thus,

$$\begin{aligned} \text{Cov}[Y_t, X_t \mid \mathcal{F}_{t-1}] &= \text{Cov}[Y_t, (z + m_{t-1})Y_t \mid \mathcal{F}_{t-1}] \\ &= \text{Cov}[Y_t, zY_t \mid \mathcal{F}_{t-1}] + m_{t-1} \text{Var}[Y_t \mid \mathcal{F}_{t-1}]. \end{aligned}$$

To handle the first term, note that

$$\mathbb{E}[zY_t \mid \mathcal{F}_{t-1}] = 0 \quad \text{and} \quad \mathbb{E}[zY_t^2 \mid \mathcal{F}_{t-1}] = 0$$

because zY_t and zY_t^2 are odd in the (conditionally) symmetric variable z . Hence

$$\text{Cov}[Y_t, zY_t \mid \mathcal{F}_{t-1}] = \mathbb{E}[zY_t^2 \mid \mathcal{F}_{t-1}] - \mathbb{E}[Y_t \mid \mathcal{F}_{t-1}] \mathbb{E}[zY_t \mid \mathcal{F}_{t-1}] = 0,$$

and therefore

$$\text{Cov}[Y_t, X_t \mid \mathcal{F}_{t-1}] = m_{t-1} \text{Var}[Y_t \mid \mathcal{F}_{t-1}].$$

Conclude. Plugging this into (3) gives

$$\Delta \text{Var}_t = \beta_1^2 m_{t-1}^2 \text{Var}[Y_t \mid \mathcal{F}_{t-1}] + 2\beta_1(1 - \beta_1)m_{t-1} \text{Cov}[Y_t, X_t \mid \mathcal{F}_{t-1}] = (2\beta_1 - \beta_1^2)m_{t-1}^2 \text{Var}[Y_t \mid \mathcal{F}_{t-1}].$$

Finally, since $\text{Var}[Y_t \mid \mathcal{F}_{t-1}] \geq 0$ and $2\beta_1 - \beta_1^2 = \beta_1(2 - \beta_1) \geq 0$ for $\beta_1 \in [0, 1]$, we obtain $\Delta \text{Var}_t \geq 0$, as claimed. \square

B.2 Proof of Theorem 3.2

Proof. We work coordinate-wise (all operations are element-wise), so it suffices to consider the scalar case. Let $u \neq 0$ be fixed, $g_0 = Mu$ with $M \gg 1$, and $g_t = u$ for all $t \geq 1$. Assume $\Delta_{-1} = 0$ and $m_{-1} = 0$, and $v_{-1} = s_{-1} = \bar{d} > 0$.

Part I: LaProp and MVN-Grad are uniformly bounded in M . *LaProp (momentum after second-moment normalization).* Define

$$v_t = \beta_2 v_{t-1} + (1 - \beta_2) g_t^2, \quad z_t^{\text{LP}} := \frac{g_t}{\sqrt{v_t} + \varepsilon}, \quad \Delta_t^{\text{LP}} := \beta_1 \Delta_{t-1}^{\text{LP}} + (1 - \beta_1) z_t^{\text{LP}}.$$

At $t = 0$,

$$v_0 = \beta_2 \bar{d} + (1 - \beta_2) M^2 u^2 \geq (1 - \beta_2) M^2 u^2,$$

hence

$$|z_0^{\text{LP}}| = \frac{|Mu|}{\sqrt{v_0} + \varepsilon} \leq \frac{|Mu|}{\sqrt{(1 - \beta_2) M^2 u^2}} = \frac{1}{\sqrt{1 - \beta_2}}.$$

For $t \geq 1$, since $\sqrt{v_t} + \varepsilon \geq \varepsilon$ and $g_t = u$, we have

$$|z_t^{\text{LP}}| \leq \frac{|u|}{\varepsilon}.$$

Define

$$Z_{\text{LP}} := \max \left\{ \frac{1}{\sqrt{1 - \beta_2}}, \frac{|u|}{\varepsilon} \right\}.$$

Then $|z_t^{\text{LP}}| \leq Z_{\text{LP}}$ for all $t \geq 0$, and the recursion gives

$$|\Delta_t^{\text{LP}}| \leq \beta_1 |\Delta_{t-1}^{\text{LP}}| + (1 - \beta_1) Z_{\text{LP}} \leq \max\{|\Delta_{t-1}^{\text{LP}}|, Z_{\text{LP}}\}.$$

By induction (using $\Delta_{-1}^{\text{LP}} = 0$), $|\Delta_t^{\text{LP}}| \leq Z_{\text{LP}}$ for all $t \geq 0$, which is independent of M . *MVN-Grad (momentum after variance-style normalization).* Let

$$m_t = \beta_1 m_{t-1} + (1 - \beta_1) g_t, \quad s_t = \beta_2 s_{t-1} + (1 - \beta_2)(g_t - m_t)^2,$$

and define

$$z_t^{\text{MV}} := \frac{g_t}{\sqrt{s_t} + \varepsilon}, \quad \Delta_t^{\text{MV}} := \beta_1 \Delta_{t-1}^{\text{MV}} + (1 - \beta_1) z_t^{\text{MV}}.$$

At $t = 0$, $m_0 = (1 - \beta_1) Mu$ so $g_0 - m_0 = \beta_1 Mu$, hence

$$s_0 = \beta_2 \bar{d} + (1 - \beta_2) \beta_1^2 M^2 u^2 \geq (1 - \beta_2) \beta_1^2 M^2 u^2,$$

and therefore

$$|z_0^{\text{MV}}| = \frac{|Mu|}{\sqrt{s_0} + \varepsilon} \leq \frac{|Mu|}{\sqrt{(1 - \beta_2) \beta_1^2 M^2 u^2}} = \frac{1}{\beta_1 \sqrt{1 - \beta_2}}.$$

For $t \geq 1$, again $\sqrt{s_t} + \varepsilon \geq \varepsilon$ and $g_t = u$, giving

$$|z_t^{\text{MV}}| \leq \frac{|u|}{\varepsilon}.$$

Define

$$Z_{\text{MV}} := \max \left\{ \frac{1}{\beta_1 \sqrt{1 - \beta_2}}, \frac{|u|}{\varepsilon} \right\}.$$

The same induction argument yields $|\Delta_t^{\text{MV}}| \leq Z_{\text{MV}}$ for all $t \geq 0$. Thus we may take $C := \max\{Z_{\text{LP}}, Z_{\text{MV}}\}$, proving the uniform boundedness for LaProp and MVN-Grad.

Part II: Adam exhibits an M -growing update at some time. For Adam, with

$$m_t = \beta_1 m_{t-1} + (1 - \beta_1)g_t, \quad v_t = \beta_2 v_{t-1} + (1 - \beta_2)g_t^2, \quad \Delta_t^A := \frac{m_t}{\sqrt{v_t} + \varepsilon},$$

the closed forms (using $m_{-1} = 0, v_{-1} = \bar{d}$) are

$$\begin{aligned} m_t &= (1 - \beta_1)\beta_1^t M u + (1 - \beta_1^t)u, \\ v_t &= \beta_2^{t+1}\bar{d} + (1 - \beta_2)\beta_2^t M^2 u^2 + (1 - \beta_2^t)u^2. \end{aligned}$$

Define the index

$$t^* := \min \left\{ t \geq 1 : (1 - \beta_2)\beta_2^t M^2 u^2 \leq u^2 \right\}.$$

Then $(1 - \beta_2)\beta_2^{t^*} M^2 u^2 \leq u^2$ and hence

$$v_{t^*} \leq \beta_2^{t^*+1}\bar{d} + u^2 + (1 - \beta_2^{t^*})u^2 \leq \bar{d} + 2u^2.$$

Consequently,

$$\sqrt{v_{t^*}} + \varepsilon \leq \sqrt{\bar{d} + 2u^2} + \varepsilon =: D,$$

where D depends only on $(\beta_2, \bar{d}, u, \varepsilon)$. On the other hand,

$$|m_{t^*}| \geq (1 - \beta_1)\beta_1^{t^*} M |u| - |u|.$$

Therefore,

$$|\Delta_{t^*}^A| = \frac{|m_{t^*}|}{\sqrt{v_{t^*}} + \varepsilon} \geq \frac{(1 - \beta_1)\beta_1^{t^*} M |u| - |u|}{D}.$$

In particular, for all M large enough (depending only on $(\beta_1, \beta_2, \bar{d}, u, \varepsilon)$),

$$|\Delta_{t^*}^A| \geq \frac{|u|}{2D} (1 - \beta_1)\beta_1^{t^*} M.$$

This shows the existence of an iterate whose update grows with M . \square

B.3 Proof of Theorem 3.3

In this subsection we prove Theorem 3.3. Recall that throughout we work under Assumptions 3.1–3.2 and the following oracle model.

Assumption B.1. *Let F be L -smooth and bounded below by F_* on \mathbb{R}^d , and suppose Assumptions 3.1–3.2 hold. In addition, assume a high-SNR stochastic oracle: we observe $g_t = \nabla F(x_{t-1}) + \xi_t$ such that $\mathbb{E}[\xi_t | \mathcal{F}_{t-1}] = 0$ and, for some $\delta \in (0, 1)$ and $\sigma \geq 0$,*

$$|\xi_{t,i}| \leq \delta |\nabla_i F(x_{t-1})| \quad a.s., \quad \mathbb{E}[\xi_{t,i}^2 | \mathcal{F}_{t-1}] \leq \sigma^2,$$

for all $i \in [d]$ and $t \geq 1$.

The proof proceeds in two steps: we first establish the convergence rate for MVN-Grad under the above assumptions, and then prove the corresponding lower bound for LaProp.

MVN-Grad: To prove the MVN-Grad part of Theorem 3.3, we first establish two auxiliary results. The first shows that, in the low-variance regime where the variance normalizer has stabilized, MVN-Grad reduces to a Heavy-Ball-type recursion driven by the stochastic oracle.

Lemma B.1. *Assume that in a low-variance phase the variance normalizer has stabilized so that $s_t \approx \sigma^2 \mathbf{1}$ for some $\sigma > 0$. Then MVN-Grad reduces to the recursion*

$$z_t = \frac{g_t}{\sigma}, \quad u_t = \beta_1 u_{t-1} + (1 - \beta_1) z_t, \quad x_t = x_{t-1} - \eta u_t,$$

Eliminating u_{t-1} yields, for all $t \geq 1$,

$$x_t = x_{t-1} + \beta(x_{t-1} - x_{t-2}) - \alpha g_t, \quad \alpha := \eta(1 - \beta) \frac{1}{\sigma}, \quad (4)$$

where we take $x_{-1} := x_0$ (equivalently $v_0 := 0$).

Proof. From $x_{t-1} = x_{t-2} - \eta u_{t-1}$ we have $u_{t-1} = -(x_{t-1} - x_{t-2})/\eta$. Using $u_t = \beta u_{t-1} + (1 - \beta) \frac{g_t}{\sigma}$ gives

$$x_t = x_{t-1} - \eta u_t = x_{t-1} + \beta(x_{t-1} - x_{t-2}) - \eta(1 - \beta) \frac{g_t}{\sigma},$$

which is (4). \square

Lemma B.1 reduces the analysis of MVN-Grad in the stabilized low-variance regime to a Heavy-Ball recursion with an additive stochastic driving term. The next lemma introduces a suitable potential function and establishes a one-step descent inequality, which we will later telescope to obtain the claimed rate.

Lemma B.2. *Define the increments $y_t := x_t - x_{t-1}$ for $t \geq 0$ with $y_0 := 0$, and set $\alpha := \eta(1 - \beta) \frac{1}{\sigma}$. Assume the stepsize condition*

$$\alpha \leq \frac{1 - \beta^2}{L}. \quad (5)$$

Define the potential

$$\Phi_t := F(x_t) + \frac{\beta^2}{2\alpha} \|y_t\|^2.$$

Then for all $t \geq 1$,

$$\mathbb{E}[\Phi_t | \mathcal{F}_{t-1}] \leq \Phi_{t-1} - \frac{\alpha}{2} \|\nabla F(x_{t-1})\|^2 + \frac{\alpha}{2} \mathbb{E}[\|\xi_t\|^2 | \mathcal{F}_{t-1}]. \quad (6)$$

Proof. By L -smoothness,

$$F(x_t) \leq F(x_{t-1}) + \langle \nabla F(x_{t-1}), y_t \rangle + \frac{L}{2} \|y_t\|^2. \quad (7)$$

From the definition of y_t and (4),

$$y_t + \alpha \nabla F(x_{t-1}) = \beta y_{t-1} - \alpha \xi_t.$$

Taking squared norms and expanding both sides gives

$$\|y_t\|^2 + 2\alpha \langle \nabla F(x_{t-1}), y_t \rangle + \alpha^2 \|\nabla F(x_{t-1})\|^2 = \beta^2 \|y_{t-1}\|^2 - 2\alpha\beta \langle y_{t-1}, \xi_t \rangle + \alpha^2 \|\xi_t\|^2.$$

Rearranging,

$$2\alpha \langle \nabla F(x_{t-1}), y_t \rangle = \beta^2 \|y_{t-1}\|^2 - \|y_t\|^2 - \alpha^2 \|\nabla F(x_{t-1})\|^2 + \alpha^2 \|\xi_t\|^2 - 2\alpha\beta \langle y_{t-1}, \xi_t \rangle.$$

Taking conditional expectation given \mathcal{F}_{t-1} and using $\mathbb{E}[\xi_t | \mathcal{F}_{t-1}] = 0$ (hence $\mathbb{E}[\langle y_{t-1}, \xi_t \rangle | \mathcal{F}_{t-1}] = 0$) yields

$$2\alpha \mathbb{E}[\langle \nabla F(x_{t-1}), y_t \rangle | \mathcal{F}_{t-1}] = \beta^2 \|y_{t-1}\|^2 - \mathbb{E}[\|y_t\|^2 | \mathcal{F}_{t-1}] - \alpha^2 \|\nabla F(x_{t-1})\|^2 + \alpha^2 \mathbb{E}[\|\xi_t\|^2 | \mathcal{F}_{t-1}]. \quad (8)$$

Taking conditional expectation in (7) and substituting (8) gives

$$\begin{aligned} \mathbb{E}[F(x_t) | \mathcal{F}_{t-1}] &\leq F(x_{t-1}) + \frac{\beta^2}{2\alpha} \|y_{t-1}\|^2 - \frac{1}{2\alpha} \mathbb{E}[\|y_t\|^2 | \mathcal{F}_{t-1}] - \frac{\alpha}{2} \|\nabla F(x_{t-1})\|^2 + \frac{\alpha}{2} \mathbb{E}[\|\xi_t\|^2 | \mathcal{F}_{t-1}] \\ &\quad + \frac{L}{2} \mathbb{E}[\|y_t\|^2 | \mathcal{F}_{t-1}] \\ &= F(x_{t-1}) + \frac{\beta^2}{2\alpha} \|y_{t-1}\|^2 - \frac{\alpha}{2} \|\nabla F(x_{t-1})\|^2 + \frac{\alpha}{2} \mathbb{E}[\|\xi_t\|^2 | \mathcal{F}_{t-1}] - \left(\frac{1}{2\alpha} - \frac{L}{2} \right) \mathbb{E}[\|y_t\|^2 | \mathcal{F}_{t-1}]. \end{aligned}$$

Adding $\frac{\beta^2}{2\alpha} \mathbb{E}[\|y_t\|^2 | \mathcal{F}_{t-1}]$ to both sides yields

$$\begin{aligned} \mathbb{E}\left[F(x_t) + \frac{\beta^2}{2\alpha} \|y_t\|^2 \mid \mathcal{F}_{t-1}\right] &\leq F(x_{t-1}) + \frac{\beta^2}{2\alpha} \|y_{t-1}\|^2 - \frac{\alpha}{2} \|\nabla F(x_{t-1})\|^2 + \frac{\alpha}{2} \mathbb{E}[\|\xi_t\|^2 | \mathcal{F}_{t-1}] \\ &\quad - \left(\frac{1 - \beta^2}{2\alpha} - \frac{L}{2} \right) \mathbb{E}[\|y_t\|^2 | \mathcal{F}_{t-1}]. \end{aligned}$$

Under (5), the last term is nonpositive and can be dropped. Recognizing the definition of Φ_t completes the proof. \square

Lemma B.2 introduced a one-step descent inequality. Note that by Assumption B.1, we have a.s. $\|\xi_t\|^2 = \sum_{i=1}^d \xi_{t,i}^2 \leq \delta^2 \sum_{i=1}^d (\nabla_i F(x_{t-1}))^2 = \delta^2 \|\nabla F(x_{t-1})\|^2$. Hence (6) reduces to:

$$\mathbb{E}[\Phi_t | \mathcal{F}_{t-1}] \leq \Phi_{t-1} - \frac{\alpha}{2} (1 - \delta^2) \|\nabla F(x_{t-1})\|^2.$$

Taking total expectation gives

$$\mathbb{E}[\Phi_t] \leq \mathbb{E}[\Phi_{t-1}] - \frac{\alpha}{2} (1 - \delta^2) \mathbb{E} \|\nabla F(x_{t-1})\|^2.$$

Summing from $t = 1$ to T yields

$$\frac{\alpha}{2} (1 - \delta^2) \sum_{t=1}^T \mathbb{E} \|\nabla F(x_{t-1})\|^2 \leq \mathbb{E}[\Phi_0] - \mathbb{E}[\Phi_T] \leq \mathbb{E}[\Phi_0] - F_*$$

Since $v_0 = 0$, $\Phi_0 = F(x_0)$. Therefore,

$$\frac{\alpha}{2} (1 - \delta^2) \sum_{t=1}^T \mathbb{E} \|\nabla F(x_{t-1})\|^2 \leq F(x_0) - F_*$$

Dividing by T gives

$$\min_{0 \leq t \leq T-1} \mathbb{E} \|\nabla F(x_t)\|^2 \leq \frac{1}{T} \sum_{t=0}^{T-1} \mathbb{E} \|\nabla F(x_t)\|^2 \leq \frac{2(F(x_0) - F_*)}{\alpha(1 - \delta^2) T},$$

Finally, Jensen implies $\min_{0 \leq t \leq T-1} \mathbb{E} \|\nabla F(x_t)\| \leq \sqrt{\min_{0 \leq t \leq T-1} \mathbb{E} \|\nabla F(x_t)\|^2}$, so choosing T as stated ensures the ε -stationarity bound.

LaProp. We now prove the LaProp part of Theorem 3.3. In the small-variance regime, LaProp's second-moment normalization collapses to a (momentum-smoothed) sign method (see Section 3.3). Accordingly, we analyze the limiting sign dynamics on a smooth quadratic and show that, under the same high-SNR oracle as Assumption B.1, LaProp requires $\Omega(d/\varepsilon^2)$ iterations to reach an ε -stationary point under the standard nonconvex stepsize scale.

Objective and oracle. Throughout this proof we work with the L -smooth function

$$F(x) = \frac{L}{2} \|x\|_2^2, \quad x \in \mathbb{R}^d,$$

so that $\nabla F(x) = Lx$ and the unique stationary point is $x^* = 0$. We use the same stochastic oracle model as in Assumption B.1; in particular,

$$g_t = \nabla F(x_{t-1}) + \xi_t = Lx_{t-1} + \xi_t, \quad \mathbb{E}[\xi_t | \mathcal{F}_{t-1}] = 0, \quad |\xi_{t,i}| \leq \delta |\nabla_i F(x_{t-1})| \text{ a.s.}$$

Limiting sign-collapse dynamics. As discussed in Section 3.3, in the high-SNR small-variance regime LaProp reduces to the (stochastic) momentum-smoothed sign recursion

$$x_t = x_{t-1} - \eta_{t-1} u_{t-1}, \quad u_{t-1} := (1 - \beta) \sum_{k=0}^{t-1} \beta^{t-1-k} \text{sign}(g_{k+1}), \quad (9)$$

where $\beta \in [0, 1)$ and $\{\eta_t\}_{t \geq 0}$ is any positive stepsize sequence.

Lemma B.3. *Assume the oracle of Assumption B.1. If $x_{t-1} \succ 0$, then $\text{sign}(g_t) = \mathbf{1}$ a.s. Consequently, along any horizon for which $x_s \succ 0$ holds for all $s \leq T$, the recursion (9) coincides (a.s.) with the deterministic sign-collapse recursion*

$$x_t = x_{t-1} - \eta_{t-1} u_{t-1}, \quad u_{t-1} = (1 - \beta) \sum_{k=0}^{t-1} \beta^{t-1-k} \mathbf{1} = (1 - \beta^t) \mathbf{1}. \quad (10)$$

Proof. Fix $t \geq 1$ and coordinate j . If $x_{t-1} \succ 0$, then $x_{t-1,j} > 0$ and $\nabla_j F(x_{t-1}) = Lx_{t-1,j} > 0$. By Assumption B.1,

$$g_{t,j} = Lx_{t-1,j} + \xi_{t,j} \geq (1 - \delta)Lx_{t-1,j} > 0,$$

hence $\text{sign}(g_{t,j}) = +1$ for all j , i.e., $\text{sign}(g_t) = \mathbf{1}$ a.s. Substituting $\text{sign}(g_{k+1}) = \mathbf{1}$ into (9) yields (10). \square

Lemma B.4. *Fix any horizon $T \geq 1$, any stepsizes $\eta_0, \dots, \eta_{T-1} > 0$, and any $\beta \in [0, 1)$. Define*

$$a := \sum_{t=0}^{T-1} \eta_t (1 - \beta^{t+1}) + \frac{\eta_{T-1}}{2} (1 - \beta^T), \quad x_0 := a \mathbf{1} \in \mathbb{R}^d, \quad (11)$$

where $\mathbf{1} = (1, \dots, 1)$. Consider the recursion (9) on $F(x) = \frac{L}{2} \|x\|_2^2$ under the oracle of Assumption B.1. Then, for every $t = 0, 1, \dots, T$, the following hold almost surely:

1. **Positive orthant invariance.** $x_t \succ 0$. In particular, $\text{sign}(g_t) = \mathbf{1}$ for all $t \leq T$ a.s.

2. **Closed form.**

$$u_t = (1 - \beta^{t+1}) \mathbf{1}, \quad x_t = \left(a - \sum_{k=0}^{t-1} \eta_k (1 - \beta^{k+1}) \right) \mathbf{1}, \quad x_T = \frac{\eta_{T-1}}{2} (1 - \beta^T) \mathbf{1}.$$

3. **Gradient lower bound.**

$$\min_{0 \leq t \leq T} \|\nabla F(x_t)\|_2 = \|\nabla F(x_T)\|_2 = \frac{L}{2} (1 - \beta^T) \eta_{T-1} \sqrt{d}.$$

Equivalently, to guarantee $\min_{0 \leq t \leq T} \|\nabla F(x_t)\|_2 \leq \varepsilon$, it is necessary that

$$\eta_{T-1} \leq \frac{2\varepsilon}{L(1 - \beta^T)\sqrt{d}}. \quad (12)$$

Proof. **Positive orthant invariance.** By Lemma B.3, as long as $x_k \succ 0$ we have $\text{sign}(g_{k+1}) = \mathbf{1}$ a.s. Assume temporarily that $\text{sign}(g_{k+1}) = \mathbf{1}$ for all $k \leq t$. Then

$$u_t = (1 - \beta) \sum_{k=0}^t \beta^{t-k} \mathbf{1} = (1 - \beta^{t+1}) \mathbf{1},$$

and (9) becomes

$$x_{t+1} = x_t - \eta_t (1 - \beta^{t+1}) \mathbf{1}. \quad (13)$$

Closed form. Unrolling (13) gives, for any $t \leq T$,

$$x_t = x_0 - \sum_{k=0}^{t-1} \eta_k (1 - \beta^{k+1}) \mathbf{1} = \left(a - \sum_{k=0}^{t-1} \eta_k (1 - \beta^{k+1}) \right) \mathbf{1}.$$

Using (11), for every $t \leq T$,

$$a - \sum_{k=0}^{t-1} \eta_k (1 - \beta^{k+1}) \geq a - \sum_{k=0}^{T-1} \eta_k (1 - \beta^{k+1}) = \frac{\eta_{T-1}}{2} (1 - \beta^T) > 0,$$

so $x_t \succ 0$ for all $t \leq T$. Lemma B.3 then validates the constant-sign hypothesis, and the expression for x_T follows by plugging $t = T$.

Gradient lower bound. Since $\nabla F(x) = Lx$,

$$\|\nabla F(x_T)\|_2 = L\|x_T\|_2 = L \cdot \frac{\eta_{T-1}}{2} (1 - \beta^T) \|\mathbf{1}\|_2 = \frac{L}{2} (1 - \beta^T) \eta_{T-1} \sqrt{d}.$$

Moreover, (13) decreases each coordinate strictly while staying positive, hence $\|x_t\|_2$ (and thus $\|\nabla F(x_t)\|_2$) is strictly decreasing in t , so the minimum over $t \in \{0, \dots, T\}$ is attained at T . Finally, requiring $\|\nabla F(x_T)\|_2 \leq \varepsilon$ yields (12). \square

Theorem B.5. *Take $\eta_t = \frac{c}{L\sqrt{t+1}}$ for a constant $c > 0$, and assume T is large enough so that $1 - \beta^T \geq \frac{1}{2}$. Then there exists an initialization x_0 (given by (11)) such that the recursion (9) satisfies*

$$\min_{0 \leq t \leq T} \|\nabla F(x_t)\|_2 \geq \frac{1}{4} \cdot \frac{c\sqrt{d}}{\sqrt{T}}.$$

Hence, to guarantee $\min_{0 \leq t \leq T} \|\nabla F(x_t)\|_2 \leq \varepsilon$, it is necessary that

$$T \geq \Omega\left(\frac{d}{\varepsilon^2}\right).$$

Proof. Apply Lemma B.4 with $\eta_{T-1} = \frac{c}{L\sqrt{T}}$ and $1 - \beta^T \geq \frac{1}{2}$:

$$\min_{0 \leq t \leq T} \|\nabla F(x_t)\|_2 = \frac{L}{2} (1 - \beta^T) \eta_{T-1} \sqrt{d} \geq \frac{L}{2} \cdot \frac{1}{2} \cdot \frac{c}{L\sqrt{T}} \sqrt{d} = \frac{1}{4} \cdot \frac{c\sqrt{d}}{\sqrt{T}}.$$

Requiring the right-hand side to be at most ε yields $T = \Omega(d/\varepsilon^2)$. \square

C Experiments

C.1 MNIST experiment hyperparameters

Figure 1a.

$$\eta = 5 \cdot 10^{-3}, \quad \beta_1 = 0.999, \quad \beta_2 = 0.7, \quad \varepsilon = 10^{-8}, \quad \text{batch size} = 128.$$

Figure 1b.

$$\eta = 1 \cdot 10^{-4}, \quad \beta_1 = 0.95, \quad \beta_2 = 0.999, \quad \varepsilon = 10^{-8}, \quad \text{batch size} = 1024.$$

No optimizer-specific tuning was performed in either panel.

C.2 Single-spike robustness experiment hyperparameters

Figures 3a–3b simulate the single-spike model from Theorem 3.2 with $g_0 = Mu$ and $g_t = u$ for all $t \geq 1$, initializing the adaptive statistics with $v_{-1} = s_{-1} = \bar{d}$ and using a fixed numerical constant ε in the denominator. Within each panel, *all optimizers use identical hyperparameters*; only the spike magnitude M varies across runs.

Figure 3a (long horizon).

$$\beta_1 = 0.9, \quad \beta_2 = 0.6, \quad \varepsilon = 10^{-8}, \quad \bar{d} = 1, \quad u = 10^{-3}, \quad T = 1000.$$

Figure 3b (early carry-over regime).

$$\beta_1 = 0.99999, \quad \beta_2 = 0.1, \quad \varepsilon = 10^{-8}, \quad \bar{d} = 10, \quad u = 10, \quad T = 50.$$

No optimizer-specific tuning was performed in either panel.

C.3 CIFAR-100 with ResNet-18

Hyperparameter search. We use the same search budget across methods per batch size. For batch size 1024, we first swept $\eta \in 2 \times 10^{-3}, 3 \times 10^{-3}, 4 \times 10^{-3}$ with $\beta_1 = 0.9$ and $\beta_2 \in 0.99, 0.999$. We then swept $\beta_1 \in 0.7, 0.8, 0.9, 0.95$, and $\beta_2 \in 0.99, 0.999$ at $\eta \in 10^{-4}, 10^{-3}, 4 \times 10^{-3}, 10^{-2}$. For batch size 128, we swept $\eta \in \{10^{-4}, 5 \times 10^{-4}, 10^{-3}\}$ with $\beta_1 = 0.9$ and $\beta_2 \in \{0.99, 0.999\}$; for AdaBelief and MVN-Grad we additionally evaluate $\varepsilon_s \in \{10^{-6}, 10^{-8}\}$, while using $\varepsilon = 10^{-8}$ for all methods. We then swept $\beta_1 \in \{0.7, 0.8, 0.9, 0.95\}$ over $\eta \in \{5 \times 10^{-4}, 10^{-3}, 5 \times 10^{-3}, 10^{-2}\}$. In both cases, we perform single-seed selection followed by 3-seed evaluation.

Selected hyperparameters for CIFAR-100 / ResNet-18 For reproducibility, Tables 1–2 report results for the best configuration (by validation / selected checkpoint criterion) found in our sweep for each optimizer.

Table 6: Selected optimizer hyperparameters for CIFAR-100 / ResNet-18 (batch size 128).

Optimizer	η	β_1	β_2	ε_s
LaProp	5×10^{-4}	0.7	0.999	-
AdaBelief	1×10^{-3}	0.9	0.99	10^{-8}
Adam	5×10^{-4}	0.8	0.999	-
MVN-Grad	1×10^{-3}	0.95	0.99	10^{-8}

Table 7: Selected optimizer hyperparameters for CIFAR-100 / ResNet-18 (batch size 1024).

Optimizer	η	β_1	β_2	ε_s
AdaBelief	4×10^{-3}	0.7	0.99	10^{-8}
Adam	1×10^{-3}	0.8	0.999	-
LaProp	1×10^{-3}	0.95	0.999	-
MVN-Grad	4×10^{-3}	0.7	0.99	10^{-8}

C.4 Selected LM hyperparameters

This appendix lists the exact optimizer hyperparameters corresponding to the selected configurations reported in Tables 3 and 4. All other settings follow the training setup described in the main text.

Table 8: WikiText-103 (GPT-2 30M, seq=512, bs=128): selected optimizer hyperparameters used in Table 3.

Optimizer	η	β_1	β_2	ε_s
LaProp	1×10^{-3}	0.95	0.99	-
AdaBelief	1×10^{-3}	0.95	0.99	0
Adam	1×10^{-3}	0.95	0.99	-
MVN-Grad	1×10^{-3}	0.95	0.99	0

Table 9: OpenWebText (GPT-2 124M, block=1024): selected optimizer hyperparameters used in Table 4.

Optimizer	η	β_1	β_2	ε_s
LaPropW	1×10^{-4}	0.6	0.999	-
AdaBeliefW	1×10^{-4}	0.6	0.999	0
AdamW	1×10^{-4}	0.6	0.99	-
MVN-GradW	1×10^{-4}	0.6	0.999	0

References

[AGKS19] R. Anil, V. Gupta, T. Koren, and Y. Singer. “Memory efficient adaptive optimization”. *Advances in Neural Information Processing Systems* 32 (2019) (pages 15, 16).

[BH18] L. Balles and P. Hennig. “Dissecting adam: The sign, magnitude and variance of stochastic gradients”. In: *International Conference on Machine Learning*. PMLR. 2018, pp. 404–413 (pages 2, 15).

[BWAA18] J. Bernstein, Y.-X. Wang, K. Azizzadenesheli, and A. Anandkumar. “signSGD: Compressed optimisation for non-convex problems”. In: *International conference on machine learning*. PMLR. 2018, pp. 560–569 (page 2).

[CZTYCG18] J. Chen, D. Zhou, Y. Tang, Z. Yang, Y. Cao, and Q. Gu. “Closing the generalization gap of adaptive gradient methods in training deep neural networks”. *arXiv preprint arXiv:1806.06763* (2018) (pages 15, 16).

[CLSH18] X. Chen, S. Liu, R. Sun, and M. Hong. “On the convergence of a class of adam-type algorithms for non-convex optimization”. *arXiv preprint arXiv:1808.02941* (2018) (page 2).

[DHS11] J. Duchi, E. Hazan, and Y. Singer. “Adaptive subgradient methods for online learning and stochastic optimization.” *Journal of machine learning research* 12.7 (2011) (page 2).

[GCHKLLNZC19] B. Ginsburg, P. Castonguay, O. Hrinchuk, O. Kuchaiev, V. Lavrukhin, R. Leary, J. Li, H. Nguyen, Y. Zhang, and J. M. Cohen. “Stochastic gradient methods with layer-wise adaptive moments for training of deep networks”. *arXiv preprint arXiv:1905.11286* (2019) (pages 15, 16).

[GKS18] V. Gupta, T. Koren, and Y. Singer. “Shampoo: Preconditioned Stochastic Tensor Optimization”. In: *Proceedings of the 35th International Conference on Machine Learning*. Ed. by J. Dy and A. Krause. Vol. 80. Proceedings of Machine Learning Research. PMLR, July 2018, pp. 1842–1850. URL: <https://proceedings.mlr.press/v80/gupta18a.html> (pages 15, 16).

[HZRS16] K. He, X. Zhang, S. Ren, and J. Sun. “Deep residual learning for image recognition”. In: *Proceedings of the IEEE conference on computer vision and pattern recognition*. 2016, pp. 770–778 (page 3).

[HCOHYKUH20] B. Heo, S. Chun, S. J. Oh, D. Han, S. Yun, G. Kim, Y. Uh, and J.-W. Ha. “Adamp: Slowing down the slowdown for momentum optimizers on scale-invariant weights”. *arXiv preprint arXiv:2006.08217* (2020) (pages 15, 16).

[HSS12] G. Hinton, N. Srivastava, and K. Swersky. “Neural networks for machine learning lecture 6a overview of mini-batch gradient descent”. *Cited on* 14.8 (2012), p. 2 (page 2).

[JBJCNB] K. Jordan, Y. Jin, V. Boza, Y. Jiacheng, F. Cecista, L. Newhouse, and J. Bernstein. “Muon: An optimizer for hidden layers in neural networks, 2024”. URL https://kellerjordan.github.io/posts/muon_6/ () (pages 15, 16).

[Kar22] A. Karpathy. *nanoGPT*. <https://github.com/karpathy/nanoGPT>. GitHub repository. Accessed 2026-01-27. 2022 (page 3).

[KB14] D. P. Kingma and J. Ba. “Adam: A method for stochastic optimization”. *arXiv preprint arXiv:1412.6980* (2014) (page 2).

[KH+09] A. Krizhevsky, G. Hinton, et al. “Learning multiple layers of features from tiny images” (2009) (page 3).

[LLHLM23] H. Liu, Z. Li, D. Hall, P. Liang, and T. Ma. “Sophia: A scalable stochastic second-order optimizer for language model pre-training”. *arXiv preprint arXiv:2305.14342* (2023) (pages 3, 15, 16).

[LJHCLGH19] L. Liu, H. Jiang, P. He, W. Chen, X. Liu, J. Gao, and J. Han. “On the variance of the adaptive learning rate and beyond”. *arXiv preprint arXiv:1908.03265* (2019) (pages 3, 15, 16).

[LH+17] I. Loshchilov, F. Hutter, et al. “Fixing weight decay regularization in adam”. *arXiv preprint arXiv:1711.05101* 5.5 (2017), p. 5 (pages 3, 15, 16).

[LXLS19] L. Luo, Y. Xiong, Y. Liu, and X. Sun. “Adaptive gradient methods with dynamic bound of learning rate”. *arXiv preprint arXiv:1902.09843* (2019) (pages 15, 16).

[RWCLAS+19] A. Radford, J. Wu, R. Child, D. Luan, D. Amodei, I. Sutskever, et al. “Language models are unsupervised multitask learners”. *OpenAI blog* 1.8 (2019), p. 9 (page 3).

[RKK19] S. J. Reddi, S. Kale, and S. Kumar. “On the convergence of adam and beyond”. *arXiv preprint arXiv:1904.09237* (2019) (pages 2, 3, 15, 16).

[SS18] N. Shazeer and M. Stern. “Adafactor: Adaptive learning rates with sublinear memory cost”. In: *International Conference on Machine Learning*. PMLR. 2018, pp. 4596–4604 (pages 3, 15, 16).

[WRSSR17] A. C. Wilson, R. Roelofs, M. Stern, N. Srebro, and B. Recht. “The marginal value of adaptive gradient methods in machine learning”. *Advances in neural information processing systems* 30 (2017) (pages 2, 15).

[YGSMKM21] Z. Yao, A. Gholami, S. Shen, M. Mustafa, K. Keutzer, and M. Mahoney. “Adahessian: An adaptive second order optimizer for machine learning”. In: *proceedings of the AAAI conference on artificial intelligence*. Vol. 35. 2021, pp. 10665–10673 (pages 3, 15, 16).

[YLRHKBSDKH19] Y. You, J. Li, S. Reddi, J. Hseu, S. Kumar, S. Bhojanapalli, X. Song, J. Demmel, K. Keutzer, and C.-J. Hsieh. “Large batch optimization for deep learning: Training bert in 76 minutes”. *arXiv preprint arXiv:1904.00962* (2019) (pages 15, 16).

[YG20] W. Yuan and K.-X. Gao. “EAdam optimizer: How ε impact adam”. *arXiv preprint arXiv:2011.02150* (2020) (page 2).

[ZRSKK18] M. Zaheer, S. Reddi, D. Sachan, S. Kale, and S. Kumar. “Adaptive methods for nonconvex optimization”. *Advances in neural information processing systems* 31 (2018) (pages 3, 15, 16).

[ZZLWZY18] Z. Zhou, Q. Zhang, G. Lu, H. Wang, W. Zhang, and Y. Yu. “Adashift: Decorrelation and convergence of adaptive learning rate methods”. *arXiv preprint arXiv:1810.00143* (2018) (pages 2, 15, 16).

[ZDTD21] J. Zhuang, Y. Ding, T. Tang, N. Dvornek, S. C. Tatikonda, and J. Duncan. “Momentum centering and asynchronous update for adaptive gradient methods”. *Advances in Neural Information Processing Systems* 34 (2021), pp. 28249–28260 (page 2).

[ZTDTD20] J. Zhuang, T. Tang, Y. Ding, S. C. Tatikonda, N. Dvornek, X. Papademetris, and J. Duncan. “Adabelief optimizer: Adapting stepsizes by the belief in observed gradients”. *Advances in neural information processing systems* 33 (2020), pp. 18795–18806 (pages 2, 15, 16).

[ZWU20] L. Ziyin, Z. T. Wang, and M. Ueda. “LaProp: Separating momentum and adaptivity in Adam”. *arXiv preprint arXiv:2002.04839* (2020) (pages 2, 15, 16).